Methyltetrahydrofolate:corrinoid/iron−sulfur Protein Methyltransferase (MeTr): Protonation State of the Ligand and Active-Site Residues

Hernán Alonso,[†] Peter L. Cummins, and Jill E. Gready*

Computational Proteomics Group, John Curtin School of Medical Research, Australian National University, P.O. Box 334, Canberra ACT 2601, Australia

Received: January 8, 2009; Revised Manuscript Received: July 14, 2009

Methyltetrahydrofolate:corrinoid/iron−sulfur protein methyltransferase (MeTr) catalyzes the transfer of the N5-methyl group from N5-methyltetrahydrofolate (CH_3THF) to the cobalt center of a corrinoid/iron−sulfur protein, a reaction similar to that of cobalamin-dependent methionine synthase (MetH). For such a reaction to occur, CH_3THF is expected to be activated by a stereospecific protonation at the N5 position. It has been shown experimentally that binding to MeTr is associated with a pK_a increase and proton uptake. The enzyme could achieve this by binding the unprotonated form of CH_3THF, followed by specific protonation at the correct orientation. Here we have used computational approaches to investigate the protonation state of the ligand and active-site residues in MeTr. First, quantum mechanical (QM) methods with the PCM solvation model were used to predict protonation positions and pK_a values of pterin, folate, and their analogues in an aqueous environment. After a reliable calibration of computational and experimental results was obtained, the effect of the protein environment was then considered. Different protonation states of CH_3THF and active-site aspartic residues (D75 and D160) were investigated using QM calculations of active-site fragment complexes and the perturbed quantum atom (PQA) approach within QM/MM simulations. The final free energy results indicate that the N5 position of the tetrahydropterin ring is the preferred protonation position of CH_3THF when bound to the active site of MeTr, followed by Asp160. We also found that the active-site environment is likely to increase the pK_a of N5 by about 3 units, leading to proton uptake upon CH_3THF binding, as observed experimentally for MeTr. Some implications of the results are discussed for the MetH mechanism.

1. Introduction

The methyltetrahydrofolate:corrinoid/iron−sulfur protein methyltransferase (MeTr) enzyme was originally isolated from the acetogenic bacterium *Moorella* (formerly *Clostridium*) *thermoaceticum*.[1] This bacterium can obtain its entire carbon and energy source from CO or H_2/CO_2 by the Wood−Ljungdahl or acetyl-CoA pathway.[2−4] Initially, CO_2 is reduced to formate and converted to N5-methyltetrahydrofolate (CH_3THF) by a formate dehydrogenase and a series of tetrahydrofolate (THF) dependent enzymes. MeTr catalyzes the transfer of a methyl group from CH_3THF to the cobalt center of a corrinoid/iron−sulfur protein (C/Fe-SP). Finally, the methyl group is transferred to CO dehydrogenase/acetyl-CoA synthase (CODH/ACS),[5] which combines with a metal−CO species and CoA to form acetyl-CoA.

MeTr is different from other enzymes of the Wood−Ljungdahl pathway as it lacks metals or other prosthetic groups, and is one of the few oxygen-stable proteins.[6] Its catalysis of the reversible transfer of the N5-methyl group of CH_3THF to C/Fe-SP[7] is a reaction similar to the first half-reaction of methionine synthase.[8] The Co(I) center attacks the N5-methyl group of CH_3THF in a rate-limiting S_N2 reaction, forming an intermediate methylcob(III)amide species.

As the removal of a methyl group from a tertiary amine is not a facile reaction, even with a strong nucleophile like cob(I)amide, the N5 group of CH_3THF is expected to be activated by protonation, electrophilic coordination, or oxidation before the reaction can occur.[9] Moreover, the stereochemical characteristics of the S_N2 displacement mechanism require the proton at the N5 position to be on the opposite side of the pterin-ring plane of the CH_3THF cofactor to that from which the nucleophilic cob(I)amide approaches (i.e., from the protein and not solvent environment). The enzyme could achieve this specific arrangement by binding the unprotonated form of CH_3THF, followed by protonation when at the correct orientation.

The crystal structures of the *apo*-MeTr[10] (PDB code 1F6Y) and a MeTr·CH_3THF complex[11] (PDB code 2E7F) have been recently determined (Figure 1). The CH_3THF-binding site is located at the top of the TIM-barrel domain of the protein (Figure 2), in a polar cup-like region with several acidic residues, which is relatively solvent exposed. The pterin ring is partially buried within the TIM barrel, with most of the residues involved in pterin binding conserved among other methyl transferases and dihydropteroate synthases (DHPSs).[10] These include aspartic acid and asparagine residues (Asp43, Asn45, Asp75, Asn96, and Asp160) that form H-bond interactions with the nitrogen and oxygen atoms of the pterin ring (Figure 1).

It is expected that this array of polar residues is involved both in CH_3THF binding and also in the polarization of the pterin ring, modifying its reactivity and facilitating its protonation during the methyl-transfer reaction. The conserved residue Asp160 constitutes what has been called the "pterin hook",[10] which is present in dihydrofolate reductases and usually establishes H-bond interactions with the N2, N3, and O4 atoms of the pterin ring, either directly or through a water molecule.

* To whom correspondence should be addressed. Phone: +61 2 6125 8304. Fax: +61 2 6125 2499. E-mail: jill.gready@anu.edu.au.

[†] Molecular Plant Physiology Group, Research School of Biological Sciences, Australian National University, Canberra ACT 0200, Australia.

10.1021/jp900181g CCC: $40.75
Published on Web 10/15/2009

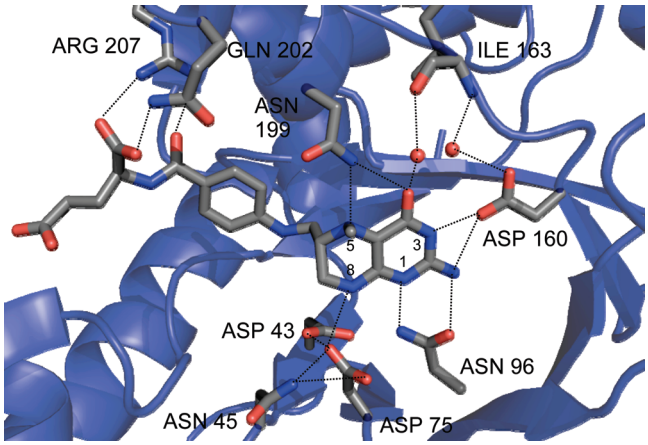

Figure 1. Disposition of the ligand methyltetrahydrofolate (CH_3THF) within the active site of MeTr. The ligand and selected active-site residues (Asp 43, Asn 45, Asp 75, Asn 96, Asp 160, Ile 163, Asn 199, Gln 202, and Arg 207) that appear to be forming H-bond interactions with the ligand are depicted in tubular form. Two crystallographic water molecules interacting with the pterin ring are shown as red spheres. Only the side chains of the residues are shown, except for Ile 163, which appears interacting with water molecules through its backbone atoms. Putative H-bond interactions are shown as dotted lines. Most of the residues involved in binding of the pterin ring (Asp43, Asp75, Asn96, and Asp160) are conserved among other methyl transferases and dihydropteroate synthases. The figure was drawn from PDB coordinates 2E7F and shows heavy atoms only (i.e., no hydrogens).

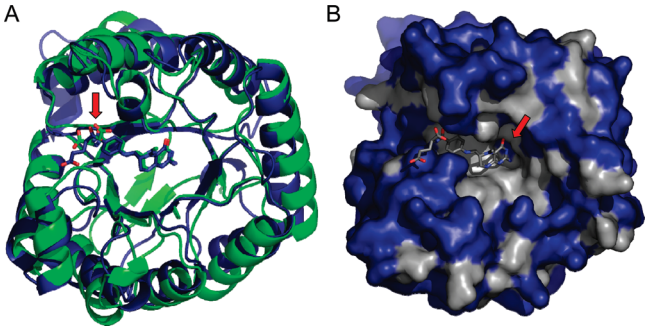

Figure 2. Structural comparison of MeTr and the CH_3THF-binding domain of MetH. (A) Superimposed structures of MeTr[11] in blue (PDB 2E7F; resolution 2.2 Å) and MetH[13] in green (PDB 1Q8J; resolution 1.9 Å). The comparison shows that the general structures of the two proteins are almost the same (Cα rmsd 1.8 Å), and that the binding conformations of the ligand CH_3THF are also strikingly similar, except for the positioning of the Glu tail (arrowed). (B) Conserved residues between MeTr and MetH (30% sequence identity, shaded in gray) mapped onto a surface representation of MeTr (blue). Most residues lining the active-site region are the same in both enzymes. The blue patch near N3 of the pterin ring (arrowed) corresponds to conservative substitutions: Ile in MeTr and Val in MetH.

While one face of the pterin ring is exposed to the solvent environment—the direction from which the cob(I)alamin cofactor is expected to approach—the other face is oriented toward the inside of the protein, which is lined by a series of nonpolar residues (I120, V194, G196, and I227), most of them conserved among methyltransferases and DHPSs. However, while in the DHPS enzymes there is a potential proton donor for the activation of the pterin ring (Lys203 in *S. aureus* DHPS, and Lys221 in *E. coli* DHPS), there is no obvious H-bond donor to the N5 atom of CH_3THF in MeTr, as the equivalent position to Lys203 in DHPS is occupied by Asn199 in MeTr. Although mutational studies of MeTr indicate that Asn199 may play an important role in stabilizing the transition state, it is not expected to activate the pterin ring by proton transfer.[11] Therefore, although specific H-bond interactions within the protein environment might increase the pK_a at the N5 position of CH_3THF, proton transfer must involve an indirect pathway.

Cobalamin-dependent methionine synthase (MetH) shares not only functional similarities with MeTr, catalyzing the methylation of a cob(I)alamin group using CH_3THF as a substrate during the methylation of homocysteine, but also presents striking structural similarities. The superposition of MeTr and the CH_3THF-binding domain of MetH (using the Dali Server[12]) gives a Cα rmsd of 1.8 Å (Figure 2) and a level of sequence identity of 30% for the superimposed residues. Interestingly, most of the active-site amino acids are absolutely conserved between the two proteins, including the asparagine residue over the N5 position that is usually occupied by a proton donor residue in the DHPS enzymes (Figure 2B).[10,13] The main difference between the two complexes is the positioning of the glutamic acid tail group of CH_3THF (Figure 2A).

Although MetH and MeTr are expected to employ an indirect strategy to protonate and activate CH_3THF, mechanisms deduced from independent experimental studies for the two systems while showing some similarities draw significantly different conclusions for the protonation. These findings are summarized in Table 1. The protonation step has been suggested to take place upon CH_3THF binding in the case of MeTr, but during a later stage, either prior to or during the methyl-transfer reaction, in the case of MetH.

For both MeTr and MetH it was found that the rate constant of the methyl-transfer reaction increases as the pH is lowered (MeTr pK_a ~5.5,[7] MetH pK_a = 5.9 ± 0.1[14]), following a pH profile that closely matches that for the N5 group of free CH_3THF (pK_a ~5).[7] However, this protonation event did not appear to affect the binding of CH_3THF to either MeTr[15] or MetH,[16] nor was it found to play a role in the activation of CH_3THF given the lack of a suitable residue at an H-bond distance from N5 that could act as direct proton donor.[14] Therefore, it was proposed that the pH dependence of the reaction was more likely to be correlated with the protonation of a general-acid/base catalyst elsewhere in the enzyme.[7]

In the case of MeTr, kinetic studies have shown that CH_3THF binds to the enzyme in the unprotonated form and then undergoes rapid protonation.[17] Furthermore, NMR studies[17] found that the pK_a of $^{13}CH_3THF$ increases by 1 pK_a unit upon binding to MeTr both in H_2O and in D_2O. The proton taken up by MeTr-bound CH_3THF is expected to originate from solvent, either directly or indirectly, as it can be measured when MeTr is titrated with CH_3THF in the presence of a pH indicator. Interestingly, although all these biochemical data indicate protonation of CH_3THF upon binding, the arrangement of hydrogen bonds in the active site of the crystal structure of MeTr·CH_3THF suggest that N5 of CH_3THF is unprotonated.[11] Doukov and co-workers[11] have suggested that the simplest explanation for this disagreement is that the rapid protonation observed in solution does not occur under the crystallization conditions used.

The lack of a direct proton donor over the N5 position of CH_3THF has led to different hypotheses regarding the mechanism of protonation/activation of the substrate, which probably follows an indirect pathway. Here we have studied the protonation and activation of the ligand CH_3THF within the MeTr active site using a computational approach. To this end, the ionization states of both the ligand and active-site aspartic acid residues were investigated in order to define the influence of the protein environment on the proton affinity of CH_3THF. Our previous experiences with the computational analysis of the

TABLE 1: Summary of Experimental Observations on the Protonation and Activation of CH_3THF within the Active Sites of MeTr and MetH

Agreement between MeTr and MetH	
Forward reaction rate (methylation of cob(I)alamin) increases as the pH is lowered, in association with an apparent pK_a of ~5.5 (MeTr)[7] or 5.9 ± 0.1 (MetH).[14]	
K_d for CH_3THF is pH independent.[15,16]	
Binding of cob(I)alamin species increases the pK_a of bound CH_3THF.[14,15]	
Reverse reaction rate (i.e., for methylation of THF using methylcobalamin as cofactor) decreases as the pH is lowered, in association with an apparent pK_a of ~5.9.[7,14]	
Disagreement	
MeTr	**MetH**
Titration of MeTr with CH_3THF (or THF) in the presence of phenol red at pH 6.8−5.2 produced changes associated with a pK_a of ~5.5−6.0.[17]	Titration of MetH with CH_3THF (or THF) in the presence of phenol red at pH 7.8 does not indicate proton uptake.[16]
^{13}C NMR studies suggest increase of 1 pK_a unit at N5 position of CH_3THF on binding enzyme.[17]	UV−visible spectral changes of CH_3THF binding to MetH over pH 8.5−5.5 indicate a decrease in pK_a at N5 (below 5).[18]
MeTr binds the protonated form of CH_3THF 10-fold stronger than the unprotonated form.[17]	Binding of protonated CH_3THF to MetH is accompanied by proton release, suggesting that the unprotonated form is the preferred ligand.[18]

protonation and reaction of dihydrofolate catalyzed by the dihydrofolate reductase (DHFR) enzyme[19−21] were central to the development of the present work.

Given the size and complexity of the system, the analysis of possible protonation profiles was carried out in a systematic, staged manner. Initially, the reliability of the computational methods to predict the protonation pattern and pK_a of several folate-like molecules in an aqueous environment was validated. Then, the size and complexity of the modeled system was increased progressively, by incorporating active-site residues and the influence of the protein environment. Protonation energies were determined initially by quantum mechanical calculations on an active-site fragment representation of the system. These studies were followed by more accurate free energy determinations using the recently described perturbed quantum atom (PQA) method within molecular dynamics (MD) simulations with a quantum mechanical (QM)/molecular mechanical (MM) potential.[22]

2. Computational Methods

2.1. Protonation Energies of Folate and Derivatives in Aqueous Environment. The potential of computational methods to estimate pK_a values for small molecules in solution has been recently highlighted by several successful reports.[23−26] To validate the reliability of QM calculations to predict both protonation positions and pK_a values, different protonated and unprotonated forms of pterin, folate, and their derivatives were analyzed (Table 2).

The molecules were manually constructed using GaussView,[27] and the final structures were optimized using Gaussian 03[28] at three different levels of theory (PM3, HF/3-21G, and HF/6-31+G**) using the PCM implicit water solvent model (IEF-PCM).[29−31]

The accuracy of both qualitative and quantitative protonation energy predictions was studied. For the qualitative analysis, relative stabilities of different protonated forms of the oxidized and reduced forms of 6-methyl-pterin and folate were calculated. The relative energies of four different sites in the pterin rings were compared, comprising N1, N5, O4, and N8. Both the ionized and the neutral forms of the pABA-Glu tail of the folate derivatives were considered.

For the quantitative analysis, protonation energies were correlated with experimentally determined pK_a's, in an approach similar to that originally published by Gready[32] and the recent study of Klamt and co-workers.[25] Several folate-like species were considered covering a pK_a range from 2.3 to 10.5 (Table 2), including some heterocyclic anions. Taking into account that the pK_a of the pABA-Glu tail of folate is ~4.5, this moiety was considered to be protonated during the QM calculations for folate (N1 pK_a = 2.35[33]) and dihydrofolate (N5 pK_a = 2.59[34]) and ionized for tetrahydrofolate (N5 pK_a = 4.82[35]) and CH_3THF (N5 pK_a = 5.05[7]).

Given that

$$pK_a = -\log(K_a) \quad \text{and} \quad \Delta G = -RT \ln K \tag{1}$$

the correlation between protonation energies and experimental pK_a values is expected to give a change of −1.36 kcal/mol per pK_a unit

$$\Delta G = -RT \ln(10) = -1.36 \text{ kcal/mol} \tag{2}$$

A similar set of HF/6-31+G** and HF/3-21G protonation energies (not shown) were generated using in vacuo QM

TABLE 2: Experimental pK_a Values and Corresponding Protonation Energies (kcal/mol) at the HF/6-31+G Level with PCM Solvent Model for a Series of Pterin-Derived Compounds**

name	site	prot. energy (kcal/mol)	exptl pK_a	ref
	Cations			
6-methyl-pterin	N1	−287.0	2.31	44
6-methyl-7,8-dihydropterin	N5	−288.9	4.17	45
6-methyl-5,6,7,8-tetrahydropterin	N5	−293.3	5.4	46
folate (FOL)	N1	−286.4	2.35	33
7,8-dihydrofolate (DHF)	N5	−286.2	2.59	34
5,6,7,8-tetrahydrofolate (THF)	N5	−292.5	4.82	35
5-methyl-5,6,7,8-tetrahydrofolate (CH_3THF)	N5	−292.2	5.05	7
6,7-dimethyl-7,8-dihydropterin	N5	−289.2	4.16	47
6,7,7-trimethyl-7,8-dihydropterin	N5	−288.7	4.24	47
	Anions			
6-methyl-pterin	N3	−307.9	8.10	44
6-methyl-5,6,7,8-tetrahydropterin	N3	−298.8	10.5	46
6-methyl-pterin 8-oxide	N3	−298.9	7.07	48
7-methyl-pterin 8-oxide	N3	−287.0	6.94	48

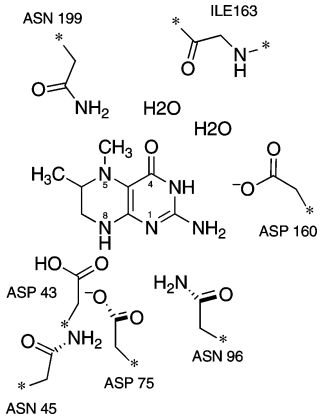

Figure 3. Schematic representation of the fragment system used to represent the active-site environment and the ligand during QM calculations. A total of 114 atoms was considered comprising the pterin-ring moiety of CH_3THF; side chains of residues D43, N45, D75, N96, D160, and N199; the backbone of residue I163; and two water molecules. Atoms marked with an asterisk were kept fixed during optimization. Different protonated forms of the pterin ring (protonated on N1, O4, N5, or N8) and residues D75 and D160 were analyzed. A total of six singly protonated and eight doubly protonated complexes were studied.

calculations. Both basis sets provided very similar results, but in contrast to the PCM calculations, molecules of different total charge were found to cluster separately. This agrees with the original work of Gready,[32] in which two different protonation plots for neutral pterin and pterin anions were constructed based on HF calculations at the STO-3G and 3-21G levels. Thus, the inclusion of the PCM implicit solvent representation not only allows calculation of protonation energies within an aqueous environment, but also permits direct comparison of molecules with different total charge within the same correlation plot.

2.2. QM Calculations on Active-Site Fragment Models. To study the effect of the protein environment on the protonation pattern and energy of the CH_3THF molecule using QM calculations, a simplified representation of the ligand and the protein active site was defined (Figure 3).

The initial coordinates of the ligand, protein side chains, and water molecules were taken from a crystal structure of the MeTr·CH_3THF complex (coordinates provided in advance of publication; now available as PDB 2E7F[11]). Optimizations were carried out at the HF/6-31G* level in vacuo (Gaussian 03[28]), and single-point in vacuo B3LYP/6-31G** calculations were performed with the final structures. In order to preserve the overall structure of the fragment close to that of the crystal structure, and to prevent unrealistic displacements of active-site groups, the Cα atoms of the side chains, as well as the terminal carbon atoms of the I163 backbone, were fixed during optimization (see Figure 3). All other atoms were free to move. Protonation of both the CH_3THF-pterin ring ($N1H^+$, $O4H^+$, $N5H^+$, and $N8H^+$) and aspartic residues (D75 and D160) were studied, comprising a total of six singly protonated and eight doubly protonated complexes. Taking into account that D43 and D75 appear within H-bond distance from each other, and that D43 is the less solvent exposed of the two, D43 was considered to be protonated in all our analyses.

For the prediction of pK_a values, single-point calculations at the HF/6-31+G** level in PCM implicit water solvent were conducted on the optimized structures, consistent with the computational level used for preparation of the calibration curve of protonation energy vs pK_a.

2.3. Free Energy Calculations Using PQA MD Simulations with QM/MM Potential. A more realistic representation of the protein environment during the protonation analysis was modeled using the perturbed quantum atom (PQA) approach in MD simulations with a QM/MM potential.[22] In this perturbative method, the protonation free energy is calculated by creating/annihilating H atoms at the positions of interest. This kind of approach was recently used by Cui and co-workers to calculate pK_a shifts for a series of small molecules in solution and their chemically related residues within protein environments.[36,37] The simulated system is divided into two regions: a semiempirical QM part, which comprises those atoms expected to have an important effect on the reaction, including those involved directly in the alchemic transformations, and an MM region, which comprises the rest of the simulated system at a lower level of accuracy. The total energy for the semiempirical QM/MM system can be written in the form

$$E = \sum_i \varepsilon_i + \sum_{i<j} \varepsilon_{ij} + \sum_{im} \varepsilon_{im} + E_{\mathrm{MM}} \qquad (3)$$

where the summations extend over all QM atoms i and j and over all MM atoms m. Thus, the first two terms account for the one-center (atomic) and two-center (diatomic) contributions to the QM energy in the semiempirical approximation, respectively, while the third, diatomic, term is the interaction energy between the QM and MM regions. The last term, E_{MM}, is the total energy associated with all atoms in the MM part of the system. In our calculations, we applied the following coupling scheme only if i was the index for a perturbed QM hydrogen:

$$\varepsilon_i + \varepsilon_j \rightarrow (1-\lambda)(\varepsilon_i + \varepsilon_j) \quad \text{and} \quad \varepsilon_{im} \rightarrow (1-\lambda)^2 \varepsilon_{im} \qquad (4)$$

Otherwise, all other ε values remained unchanged. According to eq 4, the protonated state was given by $\lambda = 0$ and the unprotonated state by $\lambda = 1$. The free energy difference between the protonated and unprotonated states was then calculated by summing energy derivatives over intermediate values of λ using the slow growth formalism:

$$\Delta G = N^{-1} \sum_{k=1}^{N} \left(\frac{\partial E}{\partial \lambda}\right)_k \quad \text{and} \quad \lambda_{k+1} = \lambda_k \pm N^{-1} \qquad (5)$$

where N is the number of MD time steps. An absolute value of the free energy for a given N was obtained as the mean of the forward (+) deprotonation and reverse (−) protonation perturbations. Convergence of this mean was then established by performing independent simulations at different values of N.

2.3.1. Preparation of Initial Structure. The X-ray coordinates of a MeTr·CH_3THF complex were provided by Dr. Doukov and Prof. Ragsdale (now available as PDB 2E7F[11]). The protein, together with six selected water molecules, was processed with the xleap module of AMBER 8.[38] Hydrogen atoms were added automatically using AMBER, and for ionizable residues the protonation states were assigned to their states at neutral pH. Although different protonation states of active-site aspartic acid residues D75 and D160 were explored during the calculations, D43 was considered to be protonated at all times. GaussView[27] was used to add H atoms to the ligand CH_3THF. Finally, the MeTr·CH_3THF complex was solvated

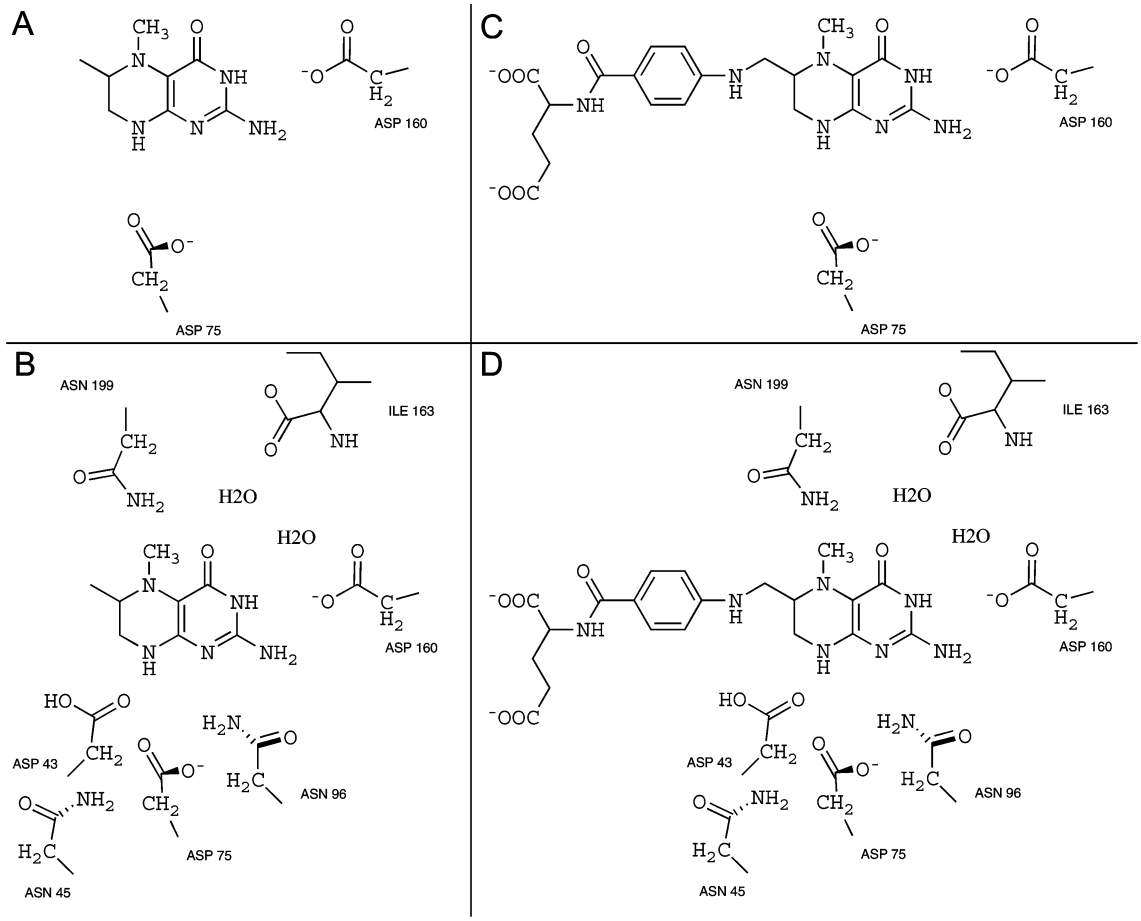

Figure 4. Schematic representations of the four different QM regions used during PQA calculations. Although the complete amino acids were included in the QM region backbone atoms are not shown (except for Ile163).

in a 38 Å radius water sphere. To maintain the integrity of the system, all water molecules between 34 and 38 Å were kept frozen during the simulations, and a constraining force was applied to keep all molecules within a 34 Å radius limit.

The system was divided into semiempirical QM and MM regions. The semiempirical QM part was treated at the PM3 semiempirical level, the MM region was simulated using the Cornell 98 force field,[39] and water molecules were described according to the TIP3P model.[40] The nonbonded electrostatic and van der Waals interactions between the QM region and the MM region were represented with a hybrid force field, as reported previously.[41−43]

2.3.2. Simulation Conditions. During the MD simulations, the value of λ was slowly increased ($\lambda = 0 \rightarrow \lambda = 1$, deprotonation) or decreased ($\lambda = 1 \rightarrow \lambda = 0$, protonation), and the free energy associated with the transformation process determined. Several simulations of different lengths were performed to ensure convergent results: eight parallel simulations of each transformation were carried out, each with a different starting velocity, and the final free energies were averaged.

A 20 Å cutoff was applied during the simulations for the electrostatic interactions within the MM region, except for interactions between charged residues, in which case there were no cutoffs. No cutoffs were used for the electrostatic interactions between the QM and the MM regions, and a 10 Å cutoff was used for all the van der Waals interactions.

During the calculations, the effect of different parameters on the final energies were considered, including the number of simulation steps during the transformation process, the size of the QM region, the polarization effect of the protein environment on the QM region, and the effect of charged MM residues. Protonation energies determined in a series of simulations ranging from 100 to 15 000 steps suggested that energy values reached convergence after 5000 steps (not shown). Therefore, simulations were carried out using λ values equivalent to 5000 steps for the larger QM regions and 10 000 steps for the smaller ones.

Four different choices of QM region were evaluated (Figure 4):

QM-A includes the pterin ring of CH_3THF and residues D75 and D75

QM-B includes the pterin ring of CH_3THF, residues D43, N45, D75, N96, D160, I163, and N199, and two crystallographic water molecules H-bonded to the pterin ring

QM-C includes the complete CH_3THF and residues D75 and D160

QM-D includes the complete CH_3THF, residues D43, N45, D75, N96, D160, I163, and N199, and two crystallographic water molecules H-bonded to the pterin ring.

To analyze the polarization effect of the protein environment, we carried out two different sets of PQA calculations. In the first, atoms within the MM region were allowed to polarize the QM atoms, whereas in the second polarization was not allowed. Given that the final relative protonation energies did not show significant differences, only results with polarization effects are shown.

The effect of ionizable MM residues on the final energies was also studied. In this case we compared calculations of a system with a completely neutralized MM region with those of

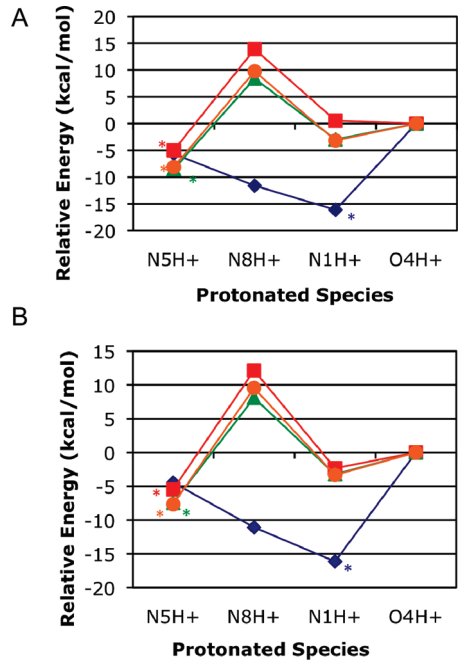

Figure 5. Protonation patterns of (A) 6-methyl-pterin (blue), 6-methyl-7,8-dihyropterin (red), 6-methyl-5,6,7,8-tetrahydropterin (green), and 5,6-dimethyl-5,6,7,8-tetrahydropterin (orange) and (B) folate (blue), dihydrofolate (red), tetrahydrofolate (green), and 5-methyl-tetrahydrofolate (orange) determined from QM energies at the HF/6-31+G** level with the PCM implicit solvent model. Relative energy values are shown using the O4-protonated species as reference. The energies shown in (B) correspond to folate and its derivatives with an ionized glutamic acid tail (−2 charge); similar results were obtained for the protonated glutamic acid (not shown). In all cases, the protonated forms with the lowest energies correspond to those found experimentally (shown by an asterisk).

a system in which the ionization states of amino acids were set according to their expected states at pH 7. Again, no significant differences were found, and only the results of the non-neutralized system are shown.

3. Results and Discussion

3.1. Protonation Patterns and pK_a Values of Pterins and Their Folate Derivatives. To test the ability of computational methods to predict the preferred protonation positions and pK_a values of pterins and their folate derivatives in solution, QM calculations with an implicit solvent representation were carried out.

Initially, the relative energies of different protonated forms of 6-methyl-pterin and folate, including their dihydro- and tetrahydro-reduced forms, were determined at the HF/6-31+G** level with the PCM implicit solvent model. Four different protonation sites were considered (N1, N5, N8, and O4), and the final results were compared with experimentally determined values (Figure 5). In all cases, the protonated species with the lowest relative energy was that found experimentally; similar results were obtained at the B3LYP level (results not shown). Thus we concluded that protonation energies obtained at the HF/6-31+G** PCM level can be used to reliably predict the preferred protonation site of pterin-like molecules.

The ability to predict not only the position but also the pK_a of the protonatable group was next tested. Several pterin-derived compounds with experimentally determined pK_a's were analyzed, covering a pK_a range from 2.3 to 10.5 (Table 2), in an approach similar to that originally published by Gready[32] and the recent work of Klamt and co-workers.[25] The protonation

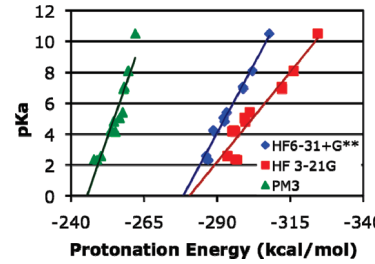

Figure 6. Correlations between experimentally determined pK_a values and protonation energies calculated at different QM levels using PCM implicit solvation conditions. Compounds included in the correlations are given in Table 2. The final correlations are −2.84 kcal/mol per pK_a unit for HF/6-31G** ($R^2 = 0.97$), −4.31 kcal/mol per pK_a unit for HF/3-21G ($R^2 = 0.90$), and −1.85 kcal/mol per pK_a unit for PM3 ($R^2 = 0.88$).

energies were determined at different QM levels (PM3, HF/6-31G, and HF/6-31+G**), with and without the PCM solvation model; results for the former are shown in Figure 6.

All computational regimes produced accurate correlations between protonation energies and experimentally determined pK_a values. The HF/6-31G** PCM energies show the best linear fit, with an R^2 value of 0.97, whereas the PM3 energies give a slope of −1.85 kcal/mol per pK_a unit, the closest to the expected theoretical value of −1.36 kcal/mol per pK_a unit (eq 2). These values are in close agreement with those reported by Klamt and co-workers,[25] who found a correlation of 0.984 between free energies of dissociation and experimental pK_a values for 64 organic and inorganic acids calculated with the COSMO-RS method, with the slope of pK_a vs dissociation energy only 58% of the theoretically expected value. Thus we concluded that protonation energies of folate-like molecules determined at any of these levels (HF/6-31G**, HF/3-21G, and PM3) under PCM implicit solvation conditions will be adequate to predict experimental pK_a values.

Analogous calculations carried out in vacuo gave less accurate correlations, and protonated species with different total charges were found to cluster separately (results not shown). Therefore, the use of an implicit solvent model appears necessary to provide good correlations between theoretical protonation energies and experimental pK_a values, while at the same time allowing the study of molecules of different total charge within a single calibration curve.

3.2. Effect of the Protein Environment on the Protonation Properties of CH_3THF. After validating the computational predictions of protonation energies and pK_a values for different pterin-like molecules in water, the effects of the protein environment on the properties of CH_3THF were next evaluated. Two different computational approaches were employed: QM calculations on active-site fragment complexes, and free energy calculations using the PQA method within MD simulations with a QM/MM potential.

3.2.1. QM Calculations on Active-Site Fragment Complexes. To study the influence of the protein environment on the protonation pattern and pK_a of CH_3THF, a simplified fragment model of the system was constructed (Figure 3). The ligand was represented by the pterin-ring moiety of CH_3THF, 6-methyl-5,6,7,8-tetrahydropterin, and the model of the protein environment comprised only those residues that are part of the H-bonded network of the active site (side chains of D43, N45, D75, N96, D160, and N199, the backbone of I163, and two water molecules). Both singly and doubly protonated forms of the system were considered. The ionization states of two active-site aspartic residues, D75 and D160, together with four different

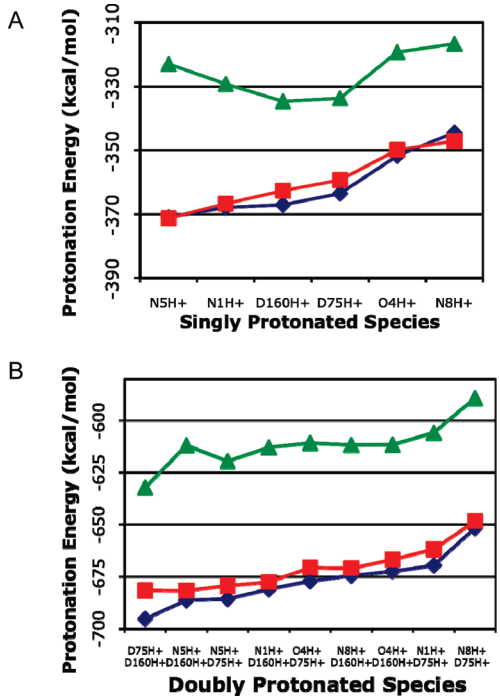

Figure 7. Single (A) and double (B) protonation energies of a fragment representation of the MeTr•CH_3THF complex. The structures (see Figure 3) were optimized at the PM3 (green) and HF/6-31G* (blue) levels. Single-point B3LYP/6-31G* (red) calculations were carried out on the HF-optimized structures. HF and B3LYP calculations show that a single proton goes preferentially to N5, as observed for the free ligand in water. PM3 energies, on the other hand, show $D160H^+$ as the most stable singly protonated species. The most stable doubly protonated species (B) appears to be $D75H^+$-$D160H^+$ (PM3, HF, and B3LYP) or $N5H^+$-$D160H^+$ (B3LYP).

protonated forms of 5,6-dimethyl-5,6,7,8-tetrahydropterin (protonated on N1, N5, N8, or O4), were systematically explored during the calculations.

All structures were optimized at the PM3 and HF/6-31G* levels, and single-point calculations were carried out at the B3LYP/6-31G* level. Final protonation energies of six singly protonated and nine doubly protonated forms of the fragment are shown in Figure 7.

HF and B3LYP single-protonation energies are nearly the same, indicating that the N5-protonated form of the system is the most stable. In the case of the PM3 calculations, although the general trend for $N8H^+$, $O4H^+$, $D75H^+$, and $D160H^+$ is similar to the ab initio results, the stability of $N1H^+$ and $N5H^+$ appears to be underestimated, and $D160H^+$ presents the most favorable protonation energy marginally over $D75H^+$. This discrepancy between the ab initio and the semiempirical results was not observed in the previous calculations of the ligand in water, suggesting that the interactions between active-site residues and the pterin-ring moiety are not properly accounted for when using the more approximate PM3 method.

In the case of the doubly protonated species, although the HF and B3LYP energies present the same general trend, the most stable structure is not the same. Whereas HF and PM3 calculations indicate that both protons will preferentially go to active-site aspartic residues D75 and D160, the B3LYP energies provide less-conclusive results. HF energies indicate that the doubly protonated form $D75H^+$-$D160H^+$ is ~9 kcal more stable than $N5H^+$-$D160H^+$, but B3LYP calculations give effectively the same energies for both species (only ~0.1 kcal difference in favor of $N5H^+$-$D160H^+$). Moreover, the B3LYP energy

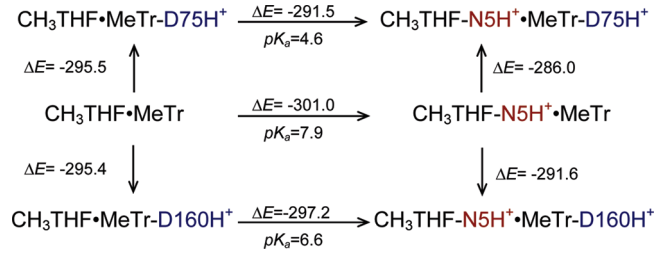

Figure 8. Protonation energies and estimated pK_a values for an active-site fragment representation of the CH_3THF•MeTr complex (see Figure 3). Protonation energies (kcal/mol) correspond to single-point HF/6-31+G** PCM calculations on the in vacuo optimized complexes (HF/6-31G*). pK_a values of N5 were estimated using the correlation shown in Figure 6.

differences for $N5H^+$-$D160H^+$, $N5H^+$-$D75H^+$, and $D75H^+$-$D160H^+$ are all quite small, suggesting that these three doubly protonated forms could coexist in the active-site environment and that more accurate calculations should be carried out to adequately predict the most stable doubly protonated form of the CH_3THF•MeTr complex.

Fragment calculations suggest that the protein environment does not alter the preferred protonation position of the ligand, which appears to be the same found in solution, i.e., N5. However, the interaction with several active-site residues might influence the effective pK_a of N5. To evaluate this, the pK_a values for the N5 position of the pterin ring within different protonated forms of the protein-fragment environment were estimated using the correlation between HF/6-31+G** PCM protonation energies and experimental pK_a values previously established (see Figure 6). These estimates are shown in Figure 8.

The HF/6-31+G** PCM protonation energies indicate that if a single proton is added to the CH_3THF•MeTr complex, it will preferentially go to N5 ($\Delta E = -301.0$ kcal/mol). The predicted pK_a for this protonation, calculated using the calibration curve shown in Figure 6, is 7.9. This value is almost 3 units higher than the experimental (and calculated) pK_a of CH_3THF in water ($pK_a = 5.0$),[7] indicating a substantial increase upon protein binding. These predictions agree with the results reported by Ragsdale and co-workers, which showed that binding of CH_3THF to MeTr is accompanied by proton uptake.[17]

Thus, although the most likely singly protonated state of the CH_3THF•MeTr complex appears to be N5-protonated CH_3THF, scenarios in which one of the active-site aspartic acid residues (D75 or D160) was already protonated were also considered. The results (Figure 8) show that binding of the CH_3THF ligand to the $D160H^+$-protonated form of the enzyme complex will result in an increase of the pK_a of N5 by ~1.6 units, whereas binding to the $D75H^+$-protonated form will make CH_3THF less basic, reducing the pK_a of N5 to 4.6. These results provide a possible explanation of the apparently conflicting results reported by Matthews and co-workers which suggested that binding of CH_3THF to MetH is accompanied by proton release rather than uptake.[18] In the case of MeTr, proton release might occur under acidic conditions (pH <5) upon binding of (presumably) protonated CH_3THF to a D75- or D160-protonated enzyme, as N5 becomes the preferred single-protonation site once the ligand is bound (Figure 8). It could also be the case that binding of the ligand to the preprotonated protein triggers a proton reshuffling, and a transfer occurs from an aspartic residue to the pterin ring without any net proton uptake from the solvent.

In summary, although the active-site environment does not affect the protonation position of the pterin ring, the aspartic

acid residues modulate the effective pH at which the protonation will occur. It is clear that if a single proton is added to the $CH_3THF \cdot MeTr$ complex, it will preferentially go to N5. Binding of the CH_3THF ligand to the ionized active site of MeTr is predicted to increase the pK_a of N5 by almost 3 units, which would result in a net proton uptake as observed by Ragsdale and co-workers.[17] Although protonation of active-site aspartic residues is unlikely to occur after binding of the ligand, a protonated *apo*-MeTr is predicted to exhibit different behavior. Formation of an N5-protonated $CH_3THF \cdot MeTr$ complex starting from a preprotonated $D75H^+$ or $D160H^+$ enzyme is likely to require proton release from the aspartic acid residues. These releases accord with the mechanism suggested by Matthews and co-workers for MetH.[18] It is possible that the apparently conflicting mechanisms arise simply from subtle differences in the active sites of MeTr and MetH which lead to different "tuning" of the basicities of the enzyme and ligand groups in the two enzymes.

As the conclusions which can be drawn from the calculations on the fragment-model representation of the $CH_3THF \cdot MeTr$ complex are limited by the simplifications of the model and availability of enthalpies only, we next carried out calculations on the reduced set of protonation possibilities indicated as most relevant so far. In these calculations, the complete ligand and complete protein environment were modeled explicitly and free energies determined by conformational sampling.

3.2.2. Free Energy Calculations Using PQA MD Simulations with QM/MM Potential. It is well-known that the active site provides a special environment for the chemical reaction to occur, modifying the reactivity of substrates and orchestrating the reaction. Although the fragment calculations allow incorporation of the effects of the active-site environment to some extent, the results suggested we needed to explore a more complete representation of the $CH_3THF \cdot MeTr$ complex. Given the presence of multiple protonatable sites in both ligand and active site, we performed more accurate free energy calculations using the perturbed quantum atom (PQA) approach.[22]

In the PQA calculations, the protonation free energy of the $CH_3THF \cdot MeTr$ complex was obtained by determining the energy associated with the creation and annihilation of a hydrogen atom. The PQA method can be implemented in such a way that the region of interest, the one undergoing the alchemic transformation, is treated at the QM level, while the rest of the system is modeled using an MM force field. Given current computational limitations, the complete ligand CH_3THF and selected active-site residues only were treated at the semiempirical PM3 level. Four different QM/MM partitions of the system were chosen (see Figure 4), and the protonation free energies of six different singly protonated species ($D160H^+$, $D75H^+$, $N5H^+$, $O4H^+$, $N1H^+$, and $N8H^+$) and eight doubly protonated forms ($N5H^+$-$D75H^+$, $N5H^+$-$D160H^+$, $O4H^+$-$D75H^+$, $O4H^+$-$D160H^+$, $N1H^+$-$D75H^+$, $N1H^+$-$D160H^+$, $N8H^+$-$D75H^+$, and $N8H^+$-$D160H^+$) were studied.

The final single-protonation free energies for the four different QM regions are shown in Figure 9.

Protonation free energies for the system with the largest QM region (QM-D) clearly predict that N5 is the preferred position for single protonation, as found for the HF fragment calculations. Although the final protonation free energies obtained with other QM/MM partitions show similar trends, none of them indicates $N5H^+$ as the most stable form. This correlates with our previous observation that the PM3 method underestimates the stability of the N5-protonated form of $CH_3THF \cdot MeTr$ in fragment calculations. However, the deficiency of the PM3 method

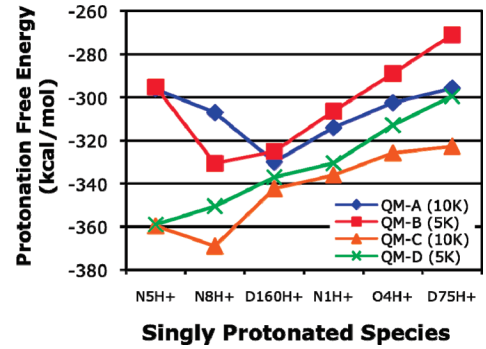

Figure 9. Single-protonation free energies of $CH_3THF \cdot MeTr$ from PQA calculations for six forms of the complex ($N5H^+$, $N8H^+$, $D160H^+$, $N1H^+$, $O4H^+$, and $D75H^+$) with four different QM/MM partitions (QM-A, QM-B, QM-C, and QM-D, see Figure 4 for details). Free energy values correspond to the average of eight independent PQA simulations (see Computational Methods). The number of steps for the transformation is shown in brackets (e.g., 10K, 10 000 steps, or $\partial\lambda = 0.0001$).

appears to become less important as the size of the QM region is increased to provide a complete and balanced description, as suggested by the results obtained with the QM-D partition showing the $N5H^+$ form as the most stable. In our simulations for dihydrofolate reductions, we have also found that it is necessary to include the complete folate cofactor in the QM region (e.g., ref 21).

When the pABA-Glu tail is removed from the QM region (QM-B), all protonation free energies become less favorable, but particularly that for the N5 site. This result suggests that the pABA-Glu tail has a particular role in stabilizing the N5-protonated form of the ligand. When the complete ligand and just the two aspartic acids, D75 and D160, are included within the QM region (QM-C), the protonation pattern does not change much, except that the $N8H^+$ form becomes the most stable. This unexpected stability of the $N8H^+$ form suggests that all active-site residues interacting with the pterin ring should be modeled reliably, as their influence appears critical to direct protonation to the N5 position of the ring. Finally, when only the pterin ring and D75 and D160 are modeled at the QM level (QM-A), the protonation trends closely follow that found for the QM-B partition except that the $N8H^+$ form is disfavored compared with the $D160H^+$ form.

To summarize, to reliably predict the preferred protonation position of the system both the complete ligand CH_3THF and all active-site residues in close proximity to the pterin ring should be modeled at the QM level. The PQA free energy calculations with the largest QM region clearly suggest that N5 is the preferred protonation position for the $CH_3THF \cdot MeTr$ complex, consistent with results from the fragment calculations.

The free energy results for the doubly protonated forms of the system are shown in Figure 10.

Protonation free energies obtained for the largest QM region, QM-D, clearly predict that the preferred doubly protonated species is $N5H^+$-$D160H^+$, in agreement with the B3LYP energy results from the fragment calculations. However, although the doubly protonated form $D75H^+$-$D160H^+$ was relatively stable according to the fragment calculations, this species is not one of the more preferred forms according to the PQA results.

A very similar protonation trend is obtained if only the complete ligand CH_3THF and the two aspartic residues D75 and D160 are included within the QM region (QM-C). However, as observed for the single-protonation calculations, the stability of $N8H^+$ appears to be overestimated and $N8H^+$-$D160H^+$ is indicated as the form with the lowest energy. This result again

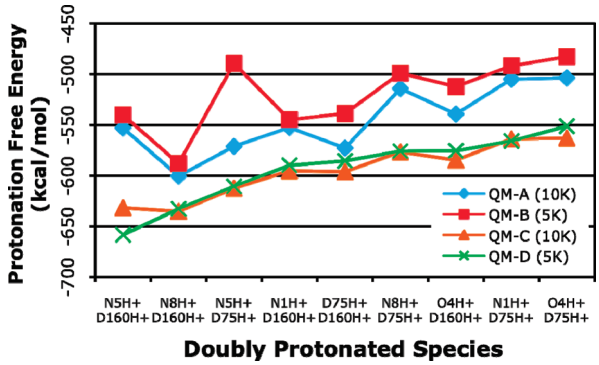

Figure 10. Double-protonation free energies of $CH_3THF \cdot MeTr$ from PQA calculations for nine doubly protonated forms of the complex ($N5H^+$-$D160H^+$, $N8H^+$-$D160H^+$, $N5H^+$-$D75H^+$, $N1H^+$-$D160H^+$, $D75H^+$-$D160H^+$, $N8H^+$-$D75H^+$, $O4H^+$-$D160H^+$, $N1H^+$-$D75H^+$, and $O4H^+$-$D75H^+$) with four different QM/MM partitions (QM-A, QM-B, QM-C, and QM-D, see Figure 4 for details). Free energy values correspond to the average of eight independent PQA simulations (see Computational Methods). The number of steps for the transformation is shown in parentheses (e.g., 10K, 10 000 steps, or $\partial\lambda = 0.0001$).

emphasizes the importance of including all active-site residues interacting with the pterin ring within the QM region to reliably predict the stability of $N5H^+$ over $N8H^+$. Omission of the pABA-Glu tail from the QM region (QM-A and QM-B) has large effects on the final free energies, destabilizing in general all doubly protonated forms, and in particular those including $N5H^+$.

To further understand the system, we performed PQA calculations with all residues within the MM region neutralized, as well as calculations in which polarization effects of the MM atoms on the QM region were ignored (data not shown). In both cases, no significant differences were found when compared with the free energy results already presented, i.e., in which QM atoms were polarized by the MM region and the ionization states of protein residues were set to those at pH 7.0.

To summarize, PQA protonation free energies obtained with the QM-D partition indicate that N5 is the preferred singly protonated form of the $CH_3THF \cdot MeTr$ complex, while $N5H^+$-$D160H^+$ is the most stable doubly protonated species. While use of more accurate ab initio calculations would provide a more reliable description, we are currently limited to use of the semiempirical PM3 method for the QM region by computational restrictions. However, based on our experience with our PM3 QM/MM simulation method and the convergence checks we have employed here, we have some confidence in the present results. The results highlight the importance of careful consideration of the QM/MM partitioning of the system. Despite the computational cost, it is clear that the QM region needs to be as complete as possible in order to obtain reliably converged results. Inclusion within the QM region of the complete ligand as well as active-site residues surrounding the pterin ring is critical for prediction of the most stable protonated form of the $CH_3THF \cdot MeTr$ complex.

4. Conclusions

We have reported a set of calculations designed to illuminate factors controlling the protonation and activation of the ligand CH_3THF within the active site of MeTr. We have concurrently considered insights from our calculations for the different protonation mechanisms proposed for MeTr and the CH_3THF-binding domain of MetH, which share significant sequence and structural homologies, from experimental studies. Although the similarity between the active sites of both enzymes and the almost identical interactions between the ligand and active-site residues suggest these two systems are likely to share a common mechanism, binding of CH_3THF to MeTr has been reported to be accompanied by an increase in the pK_a of N5 and a net proton uptake from the solvent,[17] whereas binding to MetH has been associated with a decrease in the pK_a of N5 and no proton exchange with solution.[18] Our computational study thus sought to define the most likely protonation form of CH_3THF within the MeTr active site.

Initially we validated the reliability of QM calculations to predict the protonation position and pK_a of 6-methyl-pterin derivatives, including CH_3THF, by comparison with experiments. We found that HF/6-31+G** calculations with a PCM implicit solvent representation were adequate to predict correctly the preferred protonation positions of representative pterin and folate derivatives, and to provide a good correlation between final protonation energies and experimentally determined pK_a values.

Next we tested the ability of ab initio QM calculations on active-site fragment models of the $CH_3THF \cdot MeTr$ complex, comprising only the pterin ring and several active-site residues H-bonded to it, to represent the effect of the protein environment on the protonation properties of CH_3THF. These results suggested that when a single proton is added to the system it preferentially goes to the N5 position of the 5,6-dimethyl-5,6,7,8-tetrahydropterin ring, as observed in aqueous solution. However, when two protons are added, several doubly protonated species ($N5H^+$-$D75H^+$, $N5H^+$-$D160H^+$, and $D75H^+$-$D160H^+$) show very similar energies, and it is unclear if there is a preferred form in the enzyme.

From the QM fragment calculations, we estimated that the pK_a of the N5 atom of 5,6-dimethyl-5,6,7,8-tetrahydrofolate increases by ~3 pK_a units upon binding to the unprotonated active site and, therefore, ligand binding would likely be accompanied by proton uptake, as observed by Ragsdale and co-workers.[17] Although CH_3THF is likely to be protonated before D75 or D160 in a $CH_3THF \cdot MeTr$ complex, if the ligand was to bind to a protonated form of the *apo* enzyme, then other possibilities arise. We deduced that binding of CH_3THF to MeTr-$D160H^+$ would increase the pK_a of N5 by ~1.6 units, whereas binding to a D75-protonated form of the enzyme would decrease the pK_a of N5 by ~0.4 units. If the latter applied, a proton release rather than uptake would occur, as observed by Matthews and co-workers for MetH.[18] Unfortunately, the protonation states of D160 and D75 in the *apo* forms of the two proteins are not known experimentally, but the different mechanisms can be reconciled by hypothesizing that subtle differences in the sequence/structure of MeTr and MetH lead to different basicities of the ligand groups in the two enzymes.

Finally we tested the conclusions of the fragment calculations by performing MD simulations with a QM/MM potential using the perturbed quantum atom (PQA) approach to calculate protonation free energies of the $CH_3THF \cdot MeTr$ complex. These calculations allowed modeling of the complete protein by partitioning the $CH_3THF \cdot MeTr$ complex into a high-level QM region surrounded by an MM environment. However, because of computational limitations, these simulations are possible only with a less accurate QM model, in this case the semiempirical PM3 method. These results clearly showed that N5 is the preferred protonation position of the ligand when bound to the MeTr active site, in agreement with fragment calculations, and that $N5H^+$-$D160H^+$ is the most stable doubly protonated structure. Results for several choices of QM and MM partition-

ing demonstrated that the pABA-Glu tail of CH_3THF needed to be included in the QM region, as the effect of this moiety on the protonation properties of the pterin ring was found to be more significant than the effect of surrounding active-site residues.

The fact that the PQA calculations suggest that $N5H^+$ is the most stable singly protonated form of the $CH_3THF \cdot MeTr$ complex despite the semiempirical PM3 model underestimating the protonation stability of N5 as shown by the fragment-calculation results suggests that the use of ab initio models to treat the QM region during PQA calculations would further stabilize the $N5H^+$ form.

In summary, our computational calculations indicate that the MeTr protein environment is likely to increase the pK_a of the N5 position of CH_3THF by 3 units, resulting in proton uptake upon binding to the enzyme, as observed by Ragsdale and coworkers.[17] Nevertheless, binding of the ligand to a D75- or D160-protonated form of the enzyme could result in proton release rather than uptake, as suggested by Matthews and coworkers for MetH.[18] Therefore, further protonation studies on free MeTr and MetH are needed to assess the basicities of active-site residues and correctly assign the protonation states of aspartic acids D75 and D160 in the *apo* enzymes.

Acknowledgment. We thank Dr. T. Doukov, Prof. S. Ragsdale, and Prof. C. Drennan for providing the atom coordinates of the $CH_3THF \cdot MeTr$ complex and sharing with us unpublished experimental results. We acknowledge support from the Australian Research Council (ARC) Grants DP0346292 and DP0665816, the ANU (Australian National University) IAS (Institute of Advanced Studies) block grant, and APAC (Australian Partnership for Advanced Computing) National Facility and ANU Supercomputer Facility computer-time grants.

References and Notes

(1) Drake, H. L.; Hu, S. I.; Wood, H. G. *J. Biol. Chem.* **1981**, *256*, 11137.
(2) Ljungdahl, L. G. *Annu. Rev. Microbiol.* **1986**, *40*, 415.
(3) Ragsdale, S. W. *Crit. Rev. Biochem. Mol. Biol.* **1991**, *26*, 261.
(4) Ragsdale, S. W.; Kumar, M. *Chem. Rev.* **1996**, *96*, 2515.
(5) Kumar, M.; Qiu, D.; Spiro, T. G.; Ragsdale, S. W. *Science* **1995**, *270*, 628.
(6) Roberts, D. L.; Zhao, S.; Doukov, T.; Ragsdale, S. W. *J. Bacteriol.* **1994**, *176*, 6127.
(7) Zhao, S.; Roberts, D. L.; Ragsdale, S. W. *Biochemistry* **1995**, *34*, 15075.
(8) Ludwig, M. L.; Matthews, R. G. *Annu. Rev. Biochem.* **1997**, *66*, 269.
(9) Matthews, R. G.; Banerjee, R. V.; Ragsdale, S. W. *Biofactors* **1990**, *2*, 147.
(10) Doukov, T.; Seravalli, J.; Stezowski, J. J.; Ragsdale, S. W. *Struct. Fold. Des.* **2000**, *8*, 817.
(11) Doukov, T. I.; Hemmi, H.; Drennan, C. L.; Ragsdale, S. W. *J. Biol. Chem.* **2007**, *282*, 6609.
(12) Holm, L.; Sander, C. *Methods Enzymol.* **1996**, *266*, 653.
(13) Evans, J. C.; Huddler, D. P.; Hilgers, M. T.; Romanchuk, G.; Matthews, R. G.; Ludwig, M. L. *Proc. Natl. Acad. Sci. U.S.A.* **2004**, *101*, 3729.
(14) Matthews, R. G. *Acc. Chem. Res.* **2001**, *34*, 681.
(15) Seravalli, J.; Zhao, S.; Ragsdale, S. W. *Biochemistry* **1999**, *38*, 5728.
(16) Jarrett, J. T.; Choi, C. Y.; Matthews, R. G. *Biochemistry* **1997**, *36*, 15739.
(17) Seravalli, J.; Shoemaker, R. K.; Sudbeck, M. J.; Ragsdale, S. W. *Biochemistry* **1999**, *38*, 5736.
(18) Smith, A. E.; Matthews, R. G. *Biochemistry* **2000**, *39*, 13880.
(19) Cummins, P. L.; Gready, J. E. *J. Am. Chem. Soc.* **2001**, *123*, 3418.
(20) Cummins, P. L.; Greatbanks, S. P.; Rendell, A. P.; Gready, J. E. *J. Phys. Chem. B* **2002**, *106*, 9934.
(21) Cummins, P. L.; Rostov, I. V.; Gready, J. E. *J. Chem. Theory Comput.* **2007**, *3*, 1203.
(22) Cummins, P. L.; Gready, J. E. *J. Comput. Chem.* **2005**, *26*, 561.
(23) da Silva, G.; Kennedy, E. M.; Dlugogorski, B. Z. *J. Phys. Chem. A* **2006**, *110*, 11371.
(24) Saracino, G. A. A.; Improta, R.; Barone, V. *Chem. Phys. Lett.* **2003**, *373*, 411.
(25) Klamt, A.; Eckert, F.; Diedenhofen, M.; Beck, M. E. *J. Phys. Chem. A* **2003**, *107*, 9380.
(26) Sang-Aroon, W.; Ruangpornvisuti, V. *Int. J. Quantum Chem.* **2008**, *108*, 1181.
(27) Dennington, R., II; Keith, T.; Millam, J.; Eppinnett, K.; Hovell, W. L.; Gilliland, R. *GaussView*, version 3.09; Semichem, Inc.: Shawnee Mission, KS, 2003.
(28) Frisch, M. J.; Trucks, G. W.; Schlegel, H. B.; Scuseria, G. E.; Robb, M. A.; Cheeseman, J. R.; Montgomery, J. A., Jr.; Vreven, T.; Kudin, K. N.; Burant, J. C.; Millam, J. M.; Iyengar, S. S.; Tomasi, J.; Barone, V.; Mennucci, B.; Cossi, M.; Scalmani, G.; Rega, N.; Petersson, G. A.; Nakatsuji, H.; Hada, M.; Ehara, M.; Toyota, K.; Fukuda, R.; Hasegawa, J.; Ishida, M.; Nakajima, T.; Honda, Y.; Kitao, O.; Nakai, H.; Klene, M.; Li, X.; Knox, J. E.; Hratchian, H. P.; Cross, J. B.; Bakken, V.; Adamo, C.; Jaramillo, J.; Gomperts, R.; Stratmann, R. E.; Yazyev, O.; Austin, A. J.; Cammi, R.; Pomelli, C.; Ochterski, J. W.; Ayala, P. Y.; Morokuma, K.; Voth, G. A.; Salvador, P.; Dannenberg, J. J.; Zakrzewski, V. G.; Dapprich, S.; Daniels, A. D.; Strain, M. C.; Farkas, O.; Malick, D. K.; Rabuck, A. D.; Raghavachari, K.; Foresman, J. B.; Ortiz, J. V.; Cui, Q.; Baboul, A. G.; Clifford, S.; Cioslowski, J.; Stefanov, B. B.; Liu, G.; Liashenko, A.; Piskorz, P.; Komaromi, I.; Martin, R. L.; Fox, D. J.; Keith, T.; Al-Laham, M. A.; Peng, C. Y.; Nanayakkara, A.; Challacombe, M.; Gill, P. M. W.; Johnson, B.; Chen, W.; Wong, M. W.; Gonzalez, C.; Pople, J. A. *Gaussian 03*, version C.02; Gaussian Inc.: Wallingford, CT, 2004.
(29) Mennucci, B.; Tomasi, J. *J. Chem. Phys.* **1997**, *106*, 5151.
(30) Cances, E.; Mennucci, B.; Tomasi, J. *J. Chem. Phys.* **1997**, *107*, 3032.
(31) Cossi, M.; Scalmani, G.; Rega, N.; Barone, V. *J. Chem. Phys.* **2002**, *117*, 43.
(32) Gready, J. E. *J. Comput. Chem.* **1985**, *6*, 377.
(33) Poe, M. *J. Biol. Chem.* **1977**, *252*, 3724.
(34) Maharaj, G.; Selinsky, B. S.; Appleman, J. R.; Perlman, M.; London, R. E.; Blakley, R. L. *Biochemistry* **1990**, *29*, 4554.
(35) Kallen, R. G.; Jencks, W. P. *J. Biol. Chem.* **1966**, *241*, 5845.
(36) Riccardi, D.; Schaefer, P.; Cui, Q. *J. Phys. Chem. B* **2005**, *109*, 17715.
(37) Ghosh, N.; Cui, Q. *J. Phys. Chem. B* **2008**, *112*, 8387.
(38) Case, D. A.; Darden, T. A.; Cheatham, T. E., III; Simmerling, C. L.; Wang, J.; Duke, R. E.; Luo, R.; Merz, K. M.; Wang, B.; Pearlman, D. A.; Crowley, M.; Brozell, S.; Tsui, V.; Gohlke, H.; Mongan, J.; Hornak, V.; Cui, G.; Beroza, P.; Schafmeister, C.; Caldwell, J. W.; Ross, W. S.; Kollman, P. A. *AMBER 8*; University of California: San Francisco, 2004.
(39) Cornell, W. D.; Cieplak, P.; Bayly, C. I.; Gould, I. R.; Merz, K. M.; Ferguson, D. M.; Spellmeyer, D. C.; Fox, T.; Caldwell, J. W.; Kollman, P. A. *J. Am. Chem. Soc.* **1995**, *117*, 5179.
(40) Jorgensen, W. L.; Chandrasekhar, J.; Madura, J. D.; Impey, R. W.; Klein, M. L. *J. Chem. Phys.* **1983**, *79*, 926.
(41) Cummins, P. L.; Gready, J. E. *J. Comput. Chem.* **1997**, *18*, 1496.
(42) Cummins, P. L.; Gready, J. E. *J. Comput. Chem.* **1999**, *20*, 1028.
(43) Cummins, P. L. *Molecular Orbital Programs for Simulations (MOPS)*, 1996.
(44) Braun, H.; Pfleiderer, W. *Liebigs Ann. Chem.* **1973**, 1082.
(45) Pfleiderer, W.; Zondler, H. *Chem. Ber.-Recl.* **1966**, *99*, 3008.
(46) Whiteley, J. M.; Huennekens, F. M. *Biochemistry* **1967**, *6*, 2620.
(47) Braun, H.; Pfleiderer, W. *Liebigs Ann. Chem.* **1973**, 1091.
(48) Yamamoto, H.; Hutzenlaub, W.; Pfleiderer, W. *Chem. Ber.-Recl.* **1973**, *106*, 3175.

JP900181G